



Cite this: RSC Adv., 2017, 7, 248

Facile synthesis of Prussian blue nanoparticles as pH-responsive drug carriers for combined photothermal-chemo treatment of cancer†

Huajian Chen,‡^a Yan Ma,‡^a Xianwen Wang,^a Xiaoyi Wu*^b and Zhengbao Zha*^a

Due to their clinical use approved by US Food and Drug Administration (FDA), Prussian blue nanoparticles (PB NPs) have been explored as a new generation of photothermal agents for cancer photothermal therapy (PTT). However, PTT treatment alone has limited therapeutic efficiency since it can not eliminate tumor cells completely. Herein we developed a facile method for the synthesis of PB NPs through a combined ligand exchange and thin film hydration process, modified the PB NPs by lipid-PEG conjugation, producing PEGylated PB NPs, and encapsulated doxorubicin (DOX) in the PEGylated PB NPs *via* hydrophobic interactions, creating PEGylated PB-DOX NPs. Obtained from the results of fluorescence intensity measurements, the loading efficiency and content of DOX in PEGylated PB-DOX NPs was as high as 98.0% and 9.2%, respectively. The DOX release from the PEGylated PB-DOX NPs was significantly enhanced at acidic pH, likely due to the protonation of the amine group, and a three-parameter simulation model was used to gain insight into the pH effect on DOX release. Moreover, a cell cytotoxicity study *in vitro* shows that PEGylated PB-DOX NPs exhibits a remarkable photothermal-chemo synergistic effect to HeLa cells, attributed to both photothermal ablation mediated by the PEGylated PB NPs and enhanced cellular uptake of DOX. Therefore, our study may open a new path for the production of PB NPs as drug delivery vehicles for combined photothermal-chemo cancer treatment.

Received 9th October 2016
 Accepted 27th October 2016

DOI: 10.1039/c6ra24979e
www.rsc.org/advances

Introduction

Malignant tumors (cancer) with high recurrence rates are considered to be one of the most serious health issues due to their multilevel intricacies and vast diversity in genetic content, protein expression and cellular/tissue microenvironment.^{1–3} Comparing to conventional cancer-therapeutic modalities (*e.g.* surgery, chemotherapy and radiotherapy), the burgeoning photothermal therapy (PTT), which could “cook” cancer cells using heat transferred from absorbed light energy (especially near-infrared (NIR, $\lambda = 700\text{--}1000\text{ nm}$) light), has received increasing attention owing to their unique advantages, such as localized cell-killing ability and remote controllability.^{4,5} However, the limitation is that PTT only can partially eradicate tumor, because of inhomogeneous heat distribution with tumor tissue.^{6,7} It has been proposed that combining PTT with chemotherapy may induce a synergistic effect in comparison to

sole treatment.⁸ Subsequently, various NIR-absorbing nano-materials, such as gold nanostructures,^{9–11} carbon-based nano-materials,^{12–16} copper sulfide nanoparticles,^{6,17,18} palladium nanosheets,¹⁹ transition-metal dichalcogenides nanosheets (*e.g.*, MoS₂, WS₂, *etc.*),^{20,21} and a number of organic polymers nanoparticles,^{22–25} have been developed as drug delivery vehicles for combined photothermal-chemo treatment of cancer cells.

Prussian blue (PB), a prototype of mixed-valence transition metal hexacyanoferrates, is considered as one of the earliest developed metal-organic frameworks (MOFs) with a distinct blue color.²⁶ As a US Food and Drug Administration (FDA) approved material with good biosafety, PB has gained wide clinical acceptance for use to reverse the damage of excess radiation.²⁷ Very recently, PB nanoparticles (PB NPs) have been explored as a new generation of NIR-laser driven PTT agent for cancer cell ablation owing to their high absorbance in the NIR window.^{28–30} For instance, several theranostic systems based on PB NPs have been developed, such as Fe₃O₄@PB NPs for improved magnetic resonance imaging and PTT,³¹ Au@PB NPs for dual mode photoacoustic/CT imaging and PTT,³² PB coated Na_{0.5}Y_{0.5}F₄:x% Lu nanocomposites for multifunctional imaging-guided PTT,³³ *etc.* Moreover, hollow and porous PB NPs with high drug payload have been developed as anticancer drug delivery vehicles for combined photothermal-chemo treatment of cancer cells with enhanced efficiency.^{34–37}

^aSchool of Biological and Medical Engineering, Hefei University of Technology, Hefei, Anhui 230009, P. R. China. E-mail: zbzha@hfut.edu.cn; Tel: +86 551 62901285

^bDepartment of Aerospace and Mechanical Engineering, Biomedical Engineering IDP, Bio5 Institute, University of Arizona, Tucson, Arizona 85721, USA. E-mail: xwu@email.arizona.edu

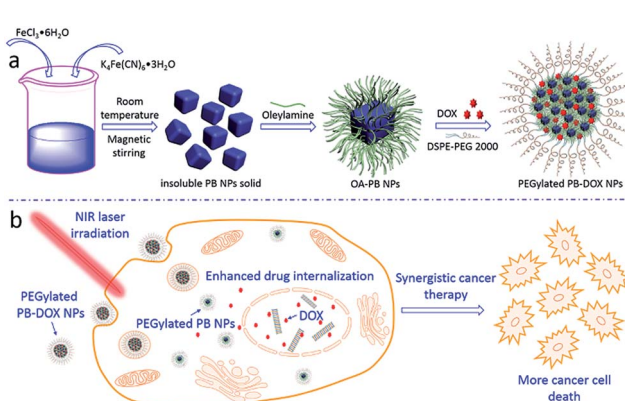
† Electronic supplementary information (ESI) available: Calculation of photothermal conversion efficiency, supplementary results. See DOI: 10.1039/c6ra24979e

‡ These authors had equal contributions for this work.



However, the production of hollow and porous PB NPs are not industrially feasible because of poor scalability along with cumbersome processes.³⁸ On the other hand, due to their limited drug loading capacity, it is still challenging to develop combined photothermal-chemo therapy based on solid PB NPs.³⁹ As well documented in literatures,^{40,41} the as-prepared insoluble PB solid synthesized from an aqueous mixture of Fe^{3+} and $[\text{Fe}^{\text{II/III}}(\text{CN})_6]^{4-3-}$ was an aggregate form of ~ 10 nm NPs. Moreover, the 3D network of cyano-bridged d- π bonding is discontinuous, and a 10 nm nanocube of PB inevitably bears 15% active surface reaction sites, $\text{Fe}(\text{III})-\text{OH}_2$, on the basis of total number of Fe.⁴¹⁻⁴³ With the help of surface modifications *via* $\text{Fe}(\text{III})-\text{OH}_2$ sites, the insoluble PB NPs solid may be transformed into dispersed solutions of PB NPs.

Therefore, in this study, we proposed a facile two-step strategy to modify the surfaces of insoluble PB NPs for applications in biomedical fields (Scheme 1a). Firstly, a simple, low-cost and high-yield synthesis of oleylamine modified PB NPs (OA-PB NPs) through surface modification of insoluble PB NPs solid with OA-toluene dispersion *via* $\text{Fe}(\text{III})-\text{OH}_2$ sites. After that, a DSPE-PEG 2000 lipid was used to coat hydrophobic OA-PB NPs through a thin-film hydration process, producing hydrophilic PEGylated PB NPs. Inspired by the synergistic effects of a combined photothermal-chemo therapy, hydrophobic doxorubicin (DOX, base form) was used as a model anticancer drug and encapsulated into hydrophobic lipid region of PEGylated PB NPs (PEGylated PB-DOX NPs). The morphologies of the as-prepared PB NPs were characterized by transmission electron microscope (TEM), and the photothermal conversion efficiency, *in vitro* drug release behavior, cell ablation efficiency were also carefully investigated. As summarized in Scheme 1b, upon NIR laser irradiation, PEGylated PB-DOX NPs would show synergistic cancer ablation effects, useful for combinational photothermal-chemo treatment of cancer cells. To the best of our knowledge, combining solid PEGylated PB NPs and DOX to improve cell-killing efficacy using this facile method has not been reported previously.



Scheme 1 Schematic illustration of (a) preparation of PEGylated PB-DOX NPs; (b) PEGylated PB-DOX NPs for combinational photothermal-chemo treatment of cancer cells.

Experimental section

Materials

$\text{FeCl}_3 \cdot 6\text{H}_2\text{O}$, $\text{K}_4\text{Fe}(\text{CN})_6 \cdot 3\text{H}_2\text{O}$ and toluene were purchased from Sinopharm Chemical Reagent Co. Ltd. Oleylamine was purchased from Aladdin. DSPE-PEG 2000 lipid was purchased from Shanghai Advanced Vehicle Technology Pharmaceutical Ltd. Doxorubicin hydrochloride (DOX·HCl) was bought from Beijing Huafeng United Technology Co. Deionized water (DI water, 18.2 M Ω cm) was used for all the experiments.

Facile synthesis of insoluble PB NPs solid

According to the published literatures,^{40,41} the insoluble PB NPs solid was precipitated as $\text{Fe}_4[\text{Fe}(\text{CN})_6]_3 \cdot 15\text{H}_2\text{O}$ from a concentrated aqueous mixture of $\text{FeCl}_3 \cdot 6\text{H}_2\text{O}$ (6.487 g, 24 mmol) and $\text{K}_4\text{Fe}(\text{CN})_6 \cdot 3\text{H}_2\text{O}$ (7.603 g, 18 mmol). After centrifugating and thoroughly washing with water and methanol, the PB NPs solid was dried under vacuum for further use.

Preparation of hydrophobic oleylamine modified PB NPs (OA-PB NPs)

To prepare the hydrophobic OA-PB NPs, the insoluble PB NPs solid (350 μg , 0.395 μmol) was dispersed in 1.0 mL DI water to form an aqueous suspension. Then, a toluene (15 mL) solution containing oleylamine (6.5 mg, 0.025 mmol) was added to the above PB NPs aqueous suspension and stirred for 30 min at room temperature. After that, centrifugation was carried out to separate the toluene and aqueous layers. Due to the good solubility of oleylamine in toluene, the as-prepared hydrophobic OA-PB NPs was successfully eluted into the toluene layer as a uniform deep-blue solution. Then the toluene layer containing OA-PB NPs was carefully taken out and stored in 4 °C for further use.

Lipid-PEGylation of PB NPs (PEGylated PB NPs)

The lipid-PEGylation of PB NPs was performed using a typical thin-film hydration method. As seen from Scheme 1a, DSPE-PEG 2000 lipid, which was dissolved in chloroform (1 mg mL⁻¹, 3.0 mL), was added to OA-PB NPs suspension in toluene (1 mg mL⁻¹, 3.0 mL), followed with gentle solvent evaporation under a nitrogen flow to form a blue thin film. After that, a predetermined amount of PBS buffer (pH = 7.4) was added to the vial and the whole system was treated with an ultrasonication process for 5 min to obtain PEGylated PB NPs aqueous solution.

Characterization of as-prepared PB NPs

The diameters of OA-PB NPs and PEGylated PB NPs were determined using a NanoBrook-90 Plus instrument (Brookhaven Instrument Corporation, Holtsville, New York, USA). The UV-vis-NIR absorption spectra of as-prepared PB NPs were obtained with a sample solution in quartz cuvette (path length: 1.0 cm) by using a spectrophotometer (U-5100, Hitachi). The morphologies of as-prepared PB NPs were acquired by



a transmission electron microscope (JEM-2100F, 200 kV accelerating voltage).

Preparation of DOX-loaded PEGylated PB NPs (PEGylated PB-DOX NPs)

Anti-cancerous model drug DOX was loaded to PEGylated PB NPs through hydrophobic interactions between hydrophobic DOX and lipid moieties (of DSPE-PEG 2000 lipid) on PB NPs. Briefly, the hydrophobic DOX in the base form was firstly prepared according to our previously published method.⁴⁴ Then, DOX and DSPE-PEG 2000 lipid at a 1 : 10 DOX-to-lipid molar ratio were mixed and dissolved in chloroform for preparing PEGylated PB-DOX NPs by using the aforementioned thin-film hydration method. Free DOX was removed from the PEGylated PB-DOX NPs solution by a typical dialysis method (dialysis bag, $M_w = 3500$, Biosharp). After that, the drug loading efficacy was calculated according to our previously reported method.⁴⁵ The drug loading content and efficiency were calculated by the following equations: loading content = (weight of drug in PEGylated PB-DOX NPs)/(weight of DSPE-PEG 2000 lipid in PEGylated PB-DOX NPs); loading efficiency = (weight of drug in PEGylated PB-DOX NPs)/(initial weight of drug).

To investigate the pH-responsive drug release profile *in vitro*, PEGylated PB-DOX NPs were incubated in PBS (0.01 mol L⁻¹, pH 4.0 and 7.4) at 37 °C and the amount of released DOX was determined by fluorescence spectrophotometry. In brief, PEGylated PB-DOX NPs (1.0 mL, 1 mg mL⁻¹), packaged in a dialysis bag ($M_w = 3500$, Biosharp), was placed in a centrifuge tube (50 mL) containing 30 mL PBS (supplemented with 0.1% v/v Tween 80) and incubated in a shaker at 37 °C. An aliquot of the release medium (3.0 mL) was withdrawn from the system and replenished with an equal volume of fresh PBS at predetermined times. The amount of released drug was quantified from fluorescent intensity (excitation = 480 nm; emission = 590 nm) using a fluorescent spectrophotometer (Hitachi F-2700). Free equivalent DOX also was dissolved in 0.75 mL DMSO plus 0.25 mL PBS and used as control. To study the influence of external NIR laser irradiation on drug release, the PEGylated PB-DOX NPs (1.0 mL, 1 mg mL⁻¹) solution was irradiated with an NIR laser (808 nm, 2.0 W) for 15 min and then a drug release experiment was carried out following the aforementioned protocol.

Numerical simulations of DOX release from PEGylated PB NPs

To gain insights into the effects of pH and laser irradiation on DOX release, a previously developed three-parameter model,⁴⁶ which considers the initial burst release and the subsequent sustained release of drug from micro- and nano-sized carriers, was fit into experimental data to obtain the release parameters of DOX. When the initial burst release and the sustained release of DOX took place at distinct time scales, the original close-form solution to the model can be simplified as follows

$$\frac{M_t}{M_0} = \frac{1}{1 + e^{-\Delta G/k_B T}} (1 - e^{-k_S t}) + \frac{e^{-\Delta G/k_B T}}{1 + e^{-\Delta G/k_B T}} (1 - e^{-k_{off} t})$$

here, M_t was the cumulative release of DOX as a function of time, M_0 was the amount of DOX that was encapsulated in PEGylated PB NPs, ΔG is a model parameter quantifying the free energy difference between the free and bound drug molecules, k_S is a model parameter defining the initial burst release, and k_{off} is a model parameter dictating the sustained release of DOX. Additionally, k_B is the Boltzmann constant, and T is the absolute temperature of solution. A MATLAB code was used in the numerical simulations of DOX release to determine ΔG , k_S , and k_{off} .

Temperature elevation of PEGylated PB NPs under NIR irradiation

Aqueous solutions of PEGylated PB NPs were irradiated with an NIR laser (808 nm, 2 W, Changchun New Industries Optoelectronics, China) for 10 min. A digital thermometer was used to monitor the solution temperature every 10 s. Moreover, according to the reported method,^{47,48} typical LASER ON/OFF cycles were used to investigate photostability and photo-thermal conversion efficiency of PEGylated PB NPs.

Photo-hyperthermic effect on cancer cells

Localized photothermal toxicity of PEGylated PB NPs was evaluated using HeLa cells (human cervical carcinoma cell line). In brief, after 24 h cultivation of HeLa cells (seeding density: 5 × 10⁴ cells per well, 24-well plate), the cells were refreshed with 400 μL PEGylated PB NPs solution (50 μg mL⁻¹ and 100 μg mL⁻¹) and locally irradiated with an NIR laser for different times (0, 3 and 5 min). After that, the cancer cells were washed with PBS buffer and treated with a live/dead assay by using calcein-AM (green fluorescence) and propidium iodide (PI, red fluorescence), respectively. According to our previously published method,⁶ a typical MTT (3-(4,5-dimethyl-2-thiazolyl)-2,5-diphenyl-2-H-tetrazolium bromide) assay was further used to quantitatively analyse the cell survival efficiency after various treatments.

Results and discussion

As seen from Fig. 1a, large quantities of insoluble PB NPs solid could be easily obtained by scaling up the coordination reaction between Fe³⁺ and [Fe(CN)₆]⁴⁻. Although the insoluble PB pigment appears to be a bulk blue powder, actually it could be considered as an aggregate form of much smaller NPs.⁴¹ Indeed, TEM analysis revealed that the PB pigment is an aggregated form of NPs of 5–20 nm in size (Fig. S1†). Two reasons may explain the formation of aggregated PB NPs. Firstly, due to the rapid consumption of Fe³⁺ and [Fe(CN)₆]⁴⁻ from the reaction solution, innumerable PB NPs would be produced at once through the rapid coordination reaction. Secondly, the neutral surface charge of insoluble PB would facilitate the aggregation precipitation even in much smaller NPs (less than 20 nm).

According to a hypothesis from reported literatures,^{49,50} if the insolubility of PB solid arises from a simple physical aggregation of smaller NPs, then PB NPs could be re-dispersed into various solvents by displacement of water ligands of Fe(III)-OH₂



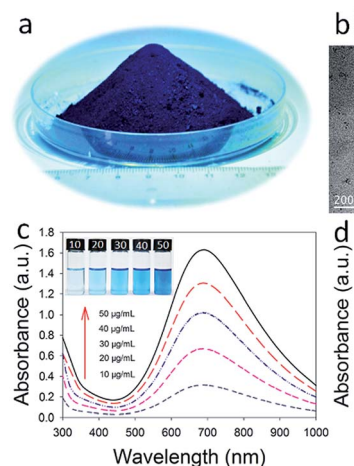


Fig. 1 Characterization of PB NPs: (a) photograph of a mass of insoluble PB NPs solid; (b) TEM image of hydrophobic OA-PB NPs; (c) UV-vis-NIR spectra of as-prepared hydrophobic OA-PB NPs with different concentrations, the inset was the photographs of as-prepared OA-PB NPs; (d) the absorbance of OA-PB NPs at 808 nm increased as the concentration of OA-PB NPs increased.

sites on the PB NPs surface. Following this synthetic strategy, oleylamine modified PB NPs (OA-PB NPs) was successfully developed by mixing the insoluble PB NPs solid with OA in toluene for 30 min. The OA-PB NPs could be stably dispersed in many organic solvents such as toluene, producing a blue solution (inset of Fig. 1c). The ultrasmall PB NPs possessed an average diameter of 8.5 ± 1.9 nm, and their good dispersity was confirmed by TEM analysis (Fig. 1b), suggesting the successful displacement of water ligands with OA molecules on the PB NPs surfaces. Due to the charge transfer from Fe(II) to Fe(III),⁵¹ the UV-vis-NIR absorption spectrum of OA-PB NPs (dispersed in toluene) showed an intense peak at 685 nm (Fig. 1c), and the absorbance at 808 nm was increased as the concentration of OA-PB NPs increased (Fig. 1d), further implying the good dispersity of OA-PB NPs in toluene.

In order to facilitate the application of OA-PB NPs as drug carrier in the biomedical field, a biocompatible DSPE-PEG 2000 lipid was used to convert the surface of PB NPs from hydrophobic into hydrophilic, and also endow the PB NPs the ability to encapsulate chemotherapeutic drugs through hydrophobic interactions. The mean hydrodynamic diameter of PEGylated PB NPs was 111 ± 25.2 nm by DLS test (Fig. S2b†), suggesting that PEGylated PB NPs were aggregates of OA-PB NPs with a lipid-PEG shell. This was further confirmed by the TEM micrographs of PEGylated PB NPs (Fig. 2a and S2a†). In a two phase system composed of toluene and water, insoluble PB NPs solid was precipitated in the bottom of the water phase due to its aggregation property. After surface ligand changed into oleylamine, the PB NPs were transferred from the aqueous phase into toluene phase (inset of Fig. 2a). Finally, the PEGylated PB NPs were dispersed very well in aqueous phase, suggesting the successful surface modification with DSPE-PEG 2000 lipid. Also, the PEGylated PB NPs possessed strong absorption in the NIR region and the absorbance linearly

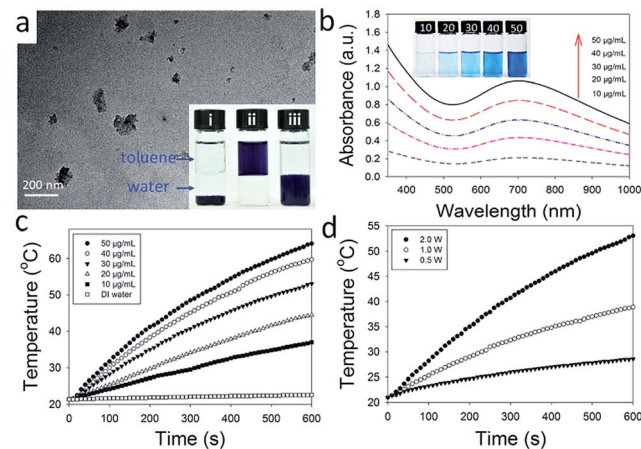


Fig. 2 Characterization of PEGylated PB NPs: (a) TEM image (inset: photographs of bare PB NPs solid, hydrophobic OA-PB NPs and PEGylated PB NPs dispersed in the mixture of toluene and water, respectively); (b) UV-vis-NIR spectra (inset: photograph of PEGylated PB NPs solution with different concentrations); (c) temperature elevation of the aqueous solution containing PEGylated PB NPs (3.0 mL) with different concentrations under NIR laser irradiation (808 nm, 2 W); (d) temperature elevation of PEGylated PB NPs ($30 \mu\text{g mL}^{-1}$, 3.0 mL) solution under NIR laser irradiation as a function of irradiation time and power density.

increased with the solution concentration of NPs (Fig. 2b and S3†), suggesting that PEGylation does not hinder the dispersity of PB NPs and its potential as a PTT agent.

Encouraged by their strong absorption in the NIR region, the photothermal conversion effect of PEGylated PB NPs was studied by irradiating 3.0 mL PEGylated PB NPs aqueous solutions with various concentrations (10, 20, 30, 40 and $50 \mu\text{g mL}^{-1}$). After being continuously exposed to NIR laser irradiation (808 nm, 2 W) for 10 min, the solution temperature was elevated from 21.4°C to 37.0°C , 44.5°C , 53.1°C , 59.7°C and 64.1°C , respectively (Fig. 2c). In sharp contrast, the temperature of DI water only increased 1.2°C . Moreover, as shown in Fig. 2d, the solution temperature increased as the laser power increased, suggesting a laser power dependent manner of temperature elevation for PEGylation PB NPs solution.

Furthermore, the photostability of PEGylated PB NPs was investigated by using five LASER ON/OFF cycles upon the help of NIR laser (808 nm, 2 W). 3.0 mL PEGylated PB NPs aqueous solution with a concentration of $30 \mu\text{g mL}^{-1}$ was used here and no significant decrease in temperature elevation was observed after five LASER ON/OFF cycles (Fig. 3a), confirming the good photostability of PEGylated PB NPs. As shown in Fig. 3b, there is no significant difference between UV-vis-NIR spectra of PEGylated PB NPs before and after five LASER ON/OFF cycles, consistent with little change in solution color (inset of Fig. 3b) and TEM images of PEGylated PB NPs solution (Fig. S4†). According to literature,⁵² the photothermal conversion efficiency also was calculated to be 36.7% for PEGylated PB NPs (Fig. 3c and d), suggesting their good potential as a photothermal agent for ablation for cancer treatment.



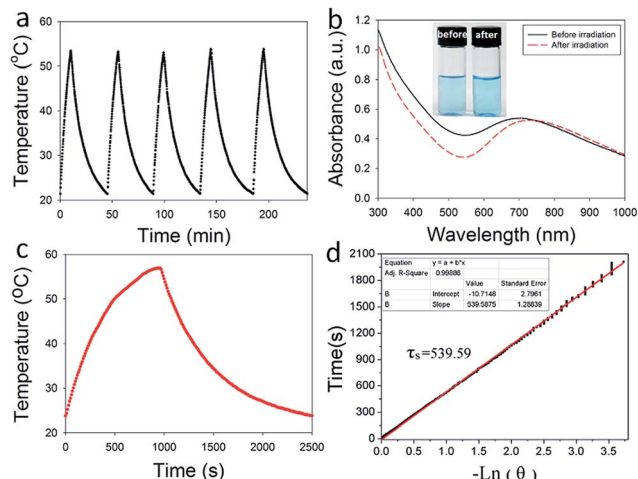


Fig. 3 (a) Temperature elevation of PEGylated PB NPs solutions under five LASER ON/OFF cycles; (b) UV-vis-NIR spectra and photographs (inset image) of PEGylated PB NPs solution before and after five LASER ON/OFF cycles, respectively; (c) the photothermal profile of a PEGylated PB NPs aqueous solution (3.0 mL, $30 \mu\text{g mL}^{-1}$) irradiated by NIR laser until reaching a steady temperature, followed by natural cooling to room temperature; (d) time constant for heat transfer of the system is determined to be $\tau_s = 539.59$ s.

To test the hypothesis that PEGylated PB NPs could be used as drug carriers for photothermal-chemo therapy, herein hydrophobic DOX in the base form as a model anticancer drug was encapsulated into PEGylated PB NPs (PEGylated PB-DOX NPs). After a typical thin-film hydration, centrifugation and washing process, PEGylated PB-DOX NPs solutions were finally obtained. Upon DOX encapsulation, the color of PEGylated PB NPs changed from blue to purple (Fig. 4b). As shown in Fig. 4a, the UV-vis-NIR spectrum of PEGylated PB-DOX NPs possesses both the characteristic absorbance of free DOX and PEGylated

PB NPs, providing a strong evidence for successful loading of DOX into the PEGylated PB NPs. According to the reported method,⁴⁵ the drug loading efficiency and content were respectively calculated to be 98.0% and 9.2% with a selected mass ratio 1 : 10 of DOX to DSPE-PEG 2000 lipid (Table S1†). Then, an *in vitro* drug release experiment was also carried out using a typical dialysis method. As shown in Fig. 4c, the release profiles of free hydrophobic DOX and PEGylated PB-DOX NPs both showed pH-dependent manners. Approximately 89.5% and 42.3% of DOX was released within 48 h at pH 4.0 for free DOX and PEGylated PB-DOX NPs, respectively. In contrast, the amount of released DOX was about 32.3% and 17.9% at pH 7.4 for free DOX and PEGylated PB-DOX NPs, suggesting that acidic pH (4.0) could enhance the release of DOX. This pH-responsive release behavior can be attributed primarily to the amine group present in DOX and DSPE-PEG 2000 lipid that protonates at low pH, rendering the drug and drug carriers hydrophilic and leading to faster release. Due to the acidic environment of cancer tissues, this pH-responsive drug release property would enhance therapeutic efficacy at tumour sites but limit the non-specific spread of toxic anticancer drugs to normal tissues with neutral pH.

On the other hand, in solutions at a pH of 7.4 or 4.0, external NIR laser irradiation (808 nm, 2.0 W, 15 min) did not induce any noticeable change in DOX release. The good thermal and mechanical stability of PEGylated PB-DOX NPs may be responsible for the insensitivity of DOX release from the drug carrier to laser irradiation. As reported by others,^{53,54} DSPE-PEG 2000 micelles have a fluid core at room temperature and do not undergo endothermic lipid chain melting transitions upon heating. Consequently, heat generated by NIR laser irradiation could not change the lipid chain structure of PEGylated PB-DOX NPs. Also the potential synergistic effect of combined photothermal-chemo therapy induced by PEGylated PB-DOX NPs may be attributed to heat-promoted NPs cellular uptake rather than heat-enhanced drug release.

To further our understanding of the effects of pH and laser irradiation on DOX release, numerical simulations using a three-parameter model were performed. As shown in Fig. 4c, the model captured DOX release from PEGylated PB NPs and free DOX. The model considers that DOX molecules are either molecularly dispersed or bound to each other and/or drug carriers. While the molecularly dispersed DOX would be rapidly released in the burst release phase, the bound DOX need to be dissociated and released at a larger time scale. The ratio of the molecularly dispersed DOX and the bound DOX is $e^{\Delta G/k_B T}$. As shown in Table S2,† when DOX was not encapsulated (*i.e.*, free DOX), $\Delta G/k_B T$ was determined to be -1.12 at pH 7.4 and $+1.36$ at pH 4.0. Accordingly, 25% DOX were molecularly dispersed at pH 7.4 and 80% at pH 4.0. The result shows that the molecular dispersion of DOX was improved in acidic conditions. When DOX was encapsulated in PEGylated PB NPs, $\Delta G/k_B T$ was determined to be -1.64 (corresponding to 16% molecularly dispersed DOX) at pH 7.4 and -0.8 (*i.e.*, 31% molecularly dispersed DOX) at pH 4.0. Therefore, in PEGylated PB NPs, acidic conditions enhance the molecular dispersion of DOX in the NPs. Further, encapsulation reduces the amount of

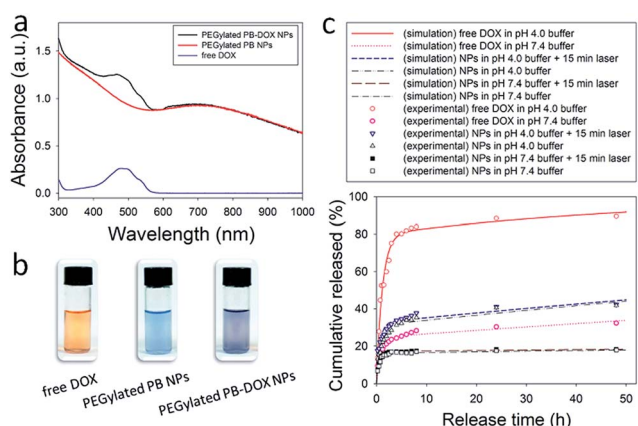


Fig. 4 (a) UV-vis-NIR spectra of PEGylated PB-DOX NPs, PEGylated PB NPs and free DOX; (b) photographs of free DOX, PEGylated PB NPs and PEGylated PB-DOX NPs solutions; (c) *in vitro* DOX release profile from PEGylated PB-DOX NPs in the PBS buffer (pH 7.4 or 4.0). Spots and lines represent results of experimental measurements and model simulations, respectively. Free DOX dissolved in DMSO was used as control.



molecularly dispersed DOX, since some drugs bind to the drug carriers. Compared to neutral conditions, acidic conditions lower k_s in both non- (0.847 h^{-1} at pH 4.0 vs. 1.137 h^{-1} at pH 7.4) and encapsulated DOX (1.025 h^{-1} at pH 4.0 vs. 1.791 h^{-1} at pH 7.4), meaning a slower burst release at pH 4.0. Taken together, the amount of the burst release increased but the rate of the burst release of DOX decreased at pH 4.0 than at neutral pH.

Compared to the profound impact of pH, laser irradiation had little effects on DOX release. In PEGylated PB-DOX NPs at pH 4.0, $\Delta G/k_B T$ slightly increased upon 5 min laser irradiation, leading to a 1.5% increase in the molecularly dispersed DOX; but a noticeable increase in k_s also was observed. This suggests that laser irradiation improves the rate but not the amount of the burst release of DOX.

An ideal photothermal agent should be non- or low-toxic for biological applications.⁵⁵ Thus, an MTT assay was performed on HUVECs to evaluate the cytotoxicity of PEGylated PB NPs. As seen from Fig. 5b, a cell viability of $85.3 \pm 3.7\%$ was achieved, after HUVECs were incubated with the solution of PEGylated PB NPs ($40 \mu\text{g mL}^{-1}$) for 24 h. The study suggests a good biocompatibility of PEGylated PB NPs. Furthermore, PEGylated PB NPs were used to treat HeLa cells under NIR light illumination to investigate their localized effects on tumor photothermal destruction. After being treated with different combinations of NPs and laser irradiation, HeLa cells were stained with calcein AM (green) and PI (red) to assess cell viability. In comparison to the negative control without PEGylated PB NPs or laser

treatment, no significant change in cell viability was identified among groups which were treated with NPs ($50 \mu\text{g mL}^{-1}$) or laser irradiation (5 min) alone (Fig. 5a). Also, no acute cell death was observed after the cells were treated with free DOX ($5 \mu\text{g mL}^{-1}$) and NIR laser irradiation (5 min). In sharp contrast, a combined treatment of HeLa cells with PEGylated PB NPs ($50 \mu\text{g mL}^{-1}$) and NIR laser illumination (5 min) led to substantial cellular death, indicating a strong photothermal destruction ability of PEGylated PB NPs. Moreover, as evident by the study, the cell destruction ability of PEGylated PB NPs depends on the illumination time and the concentration of NPs as well.

To test the synergistic effects of the combined photothermal-chemo therapy, a standard MTT assay was used to quantitatively evaluate the cytotoxicity of PEGylated PB-DOX NPs with or without NIR laser irradiation. As seen from Fig. 5c, the PEGylated PB NPs show no or little toxicity to HeLa cells without drug treatment or NIR laser irradiation, suggesting their inherent biocompatibility. When HeLa cells were treated with PEGylated PB-DOX NPs, the cell viabilities decreased as the concentration of equivalent DOX or the time of NIR laser irradiation increased (Fig. 5d and e). A concentration threshold also was identified to generate sufficient heat to kill cancer cells without the help of chemotherapeutic drug. Particularly, upon 5 min NIR light irradiation, the cell viability was 88.3% and 75.8% when HeLa cells were incubated with PEGylated PB NPs and free DOX (equivalent DOX concentration of $0.2 \mu\text{g mL}^{-1}$), respectively (Fig. 5e). Impressively, a much lower cell viability (39.2%) was achieved when the cells were treated with PEGylated PB-DOX NPs with the same equivalent DOX concentration. Specifically, the cell-killing efficacy (60.8%) of PEGylated PB-DOX NPs with laser irradiation is higher than the combined cell-killing efficacies of the photothermal therapy (11.7%) by PEGylated PB NPs and chemotherapy (24.2%) by free DOX with an equivalent concentration. At an equivalent DOX concentration that is lower than $0.5 \mu\text{g mL}^{-1}$, the heat generated upon NIR laser irradiation could not kill HeLa cells with high efficacy, but may increase cellular metabolism and membrane permeability, leading to enhanced drug uptake by cells. Therefore, our experimental findings support the potential use of PEGylated PB-DOX NPs for combinational photothermal-chemo treatment of cancer cells due to their strong synergistic effects.

Conclusions

In conclusion, a facile strategy based on ligand-exchange and thin-film hydration processes was developed for the facile synthesis of PEGylated PB NPs by coating insoluble PB NPs solid with oleylamine and then modifying OA-PB NPs with DSPE-PEG 2000 lipid. The as-prepared PEGylated PB NPs display good biocompatibility, an excellent photothermal conversion efficiency as high as 36.7%, and high absorbance in the NIR region. Utilizing hydrophobic interactions, DOX as a model anticancer drug was encapsulated into the lipid region of PEGylated PB NPs with an ultrahigh drug loading capacity and an excellent pH-responsive drug release property. Finally, our results confirmed that the as-prepared PEGylated PB-DOX NPs showed an impressive synergistic cell-killing effects on cancer cells

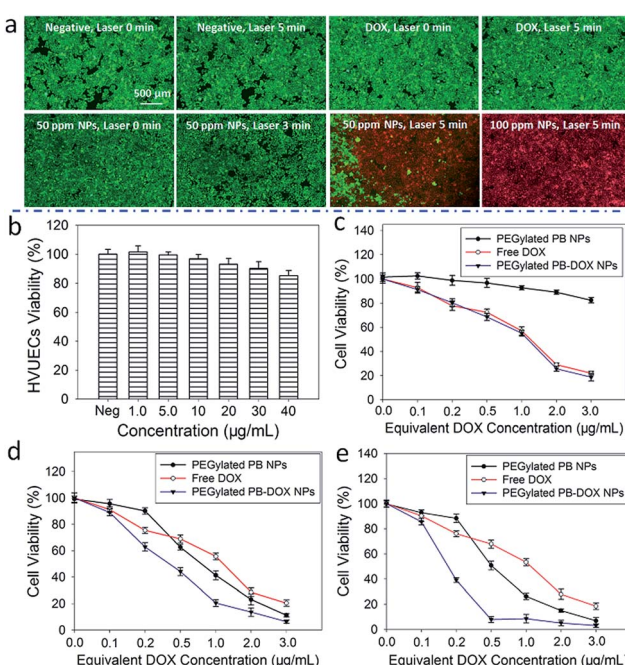


Fig. 5 (a) Localized photothermal destruction of HeLa cells treated with or without PEGylated PB NPs and NIR laser (808 nm, 2.0 W); (b) cell viability of HUVECs after 24 h exposure to various concentrations of PEGylated PB NPs; cell viability after treatment with PEGylated PB-DOX NPs and different NIR laser irradiation times (c) 0 min; (d) 3 min and (e) 5 min.



upon NIR laser irradiation, suggesting the promising potential of PEGylated PB NPs as a novel drug delivery system for combined photothermal-chemo treatments of cancer cells.

Acknowledgements

This work was financially supported by the National Natural Science Foundation of China (No. 81501590; No. 31500808), the Anhui Provincial Natural Science Foundation (No. 1608085MH188), the Fundamental Research Funds for the Central Universities (No. 2015HGCH0006; No. JZ2015HGBZ0103).

Notes and references

- 1 H. Li, R. Brescia, M. Povia, M. Prato, G. Bertoni, L. Manna and I. Moreels, *J. Am. Chem. Soc.*, 2013, **135**, 12270–12278.
- 2 S. Zhang, C. Sun, J. Zeng, Q. Sun, G. Wang, Y. Wang, Y. Wu, S. Dou, M. Gao and Z. Li, *Adv. Mater.*, 2016, **28**, 8927–8936.
- 3 A. C. Poulose, S. Veeranarayanan, M. S. Mohamed, Y. Nagaoka, R. R. Aburto, T. Mitcham, P. M. Ajayan, R. R. Bouchard, Y. Sakamoto and Y. Yoshida, *Nanoscale*, 2015, **7**, 8378–8388.
- 4 L. Zeng, L. An and X. Wu, *J. Drug Delivery*, 2011, **2011**, 370308.
- 5 Z. Zha, X. Yue, Q. Ren and Z. Dai, *Adv. Mater.*, 2013, **25**, 777–782.
- 6 Z. Zha, S. Zhang, Z. Deng, Y. Li, C. Li and Z. Dai, *Chem. Commun.*, 2013, **49**, 3455–3457.
- 7 R. Zhang, S. Su, K. Hu, L. Shao, X. Deng, W. Sheng and Y. Wu, *Nanoscale*, 2015, **7**, 19722–19731.
- 8 W. Zhang, Z. Guo, D. Huang, Z. Liu, X. Guo and H. Zhong, *Biomaterials*, 2011, **32**, 8555–8561.
- 9 T. Zheng, G. G. Li, F. Zhou, R. Wu, J. J. Zhu and H. Wang, *Adv. Mater.*, 2016, **28**, 8218–8226.
- 10 H. Chen, X. Zhang, S. Dai, Y. Ma, S. Cui, S. Achilefu and Y. Gu, *Theranostics*, 2013, **3**, 633–649.
- 11 H. Liu, D. Chen, L. Li, T. Liu, L. Tan, X. Wu and F. Tang, *Angew. Chem., Int. Ed.*, 2011, **50**, 891–895.
- 12 D. Hu, C. Liu, L. Song, H. Cui, G. Gao, P. Liu, Z. Sheng and L. Cai, *Nanoscale*, 2016, **8**, 17150–17158.
- 13 B. Guo, G. Feng, P. N. Manghnani, X. Cai, J. Liu, W. Wu, S. Xu, X. Cheng, C. Teh and B. Liu, *Small*, 2016, **12**, 6243–6254.
- 14 K. Wang, H. Yao, Y. Meng, Y. Wang, X. Yan and R. Huang, *Acta Biomater.*, 2015, **16**, 196–205.
- 15 Y. A. Cheon, J. H. Bae and B. G. Chung, *Langmuir*, 2016, **32**, 2731–2736.
- 16 R. Dou, Z. Du, T. Bao, X. Dong, X. Zheng, M. Yu, W. Yin, B. Dong, L. Yan and Z. Gu, *Nanoscale*, 2016, **8**, 11531–11542.
- 17 Z. Li, Y. Hu, M. Chang, K. A. Howard, X. Fan, Y. Sun, F. Besenbacher and M. Yu, *Nanoscale*, 2016, **8**, 16005–16016.
- 18 B. Liu, X. Zhang, C. Li, F. He, Y. Chen, S. Huang, D. Jin, P. Yang, Z. Cheng and J. Lin, *Nanoscale*, 2016, **8**, 12560–12569.
- 19 W. Fang, S. Tang, P. Liu, X. Fang, J. Gong and N. Zheng, *Small*, 2012, **8**, 3816–3822.
- 20 S. Wang, Y. Tian, W. Tian, J. Sun, S. Zhao, Y. Liu, C. Wang, Y. Tang, X. Ma, Z. Teng and G. Lu, *ACS Nano*, 2016, **10**, 8578–8590.
- 21 G. Yang, H. Gong, T. Liu, X. Sun, L. Cheng and Z. Liu, *Biomaterials*, 2015, **60**, 62–71.
- 22 X. Liu, G. Yang, L. Zhang, Z. Liu, Z. Cheng and X. Zhu, *Nanoscale*, 2016, **8**, 15323–15339.
- 23 Z. Gang, *J. Nanomed. Nanotechnol.*, 2016, **12**, 454.
- 24 M. Chen, X. Fang, S. Tang and N. Zheng, *Chem. Commun.*, 2012, **48**, 8934–8936.
- 25 M. Zheng, C. Yue, Y. Ma, P. Gong, P. Zhao, C. Zheng, Z. Sheng, P. Zhang, Z. Wang and L. Cai, *ACS Nano*, 2013, **7**, 2056–2067.
- 26 K. Itaya, T. Ataka and S. Toshima, *J. Am. Chem. Soc.*, 1982, **104**, 4767–4772.
- 27 J. Long, Y. Guarini, C. Guerin and J. Larionova, *Dalton Trans.*, 2016, **45**, 17581–17587.
- 28 G. Fu, W. Liu, S. Feng and X. Yue, *Chem. Commun.*, 2012, **48**, 11567–11569.
- 29 L. Cheng, H. Gong, W. Zhu, J. Liu, X. Wang, G. Liu and Z. Liu, *Biomaterials*, 2014, **35**, 9844–9852.
- 30 W. Zhu, K. Liu, X. Sun, X. Wang, Y. Li, L. Cheng and Z. Liu, *ACS Appl. Mater. Interfaces*, 2015, **7**, 11575–11582.
- 31 G. Fu, W. Liu, Y. Li, Y. Jin, L. Jiang, X. Liang, S. Feng and Z. Dai, *Bioconjugate Chem.*, 2014, **25**, 1655–1663.
- 32 L. Jing, X. Liang, Z. Deng, S. Feng, X. Li, M. Huang, C. Li and Z. Dai, *Biomaterials*, 2014, **35**, 5814–5821.
- 33 Y. Liu, Q. Guo, X. Zhu, W. Feng, L. Wang, L. Ma, G. Zhang, J. Zhou and F. Li, *Adv. Funct. Mater.*, 2016, **26**, 5120–5130.
- 34 M. Wu, Q. Wang, X. Liu and J. Liu, *RSC Adv.*, 2015, **5**, 30970–30980.
- 35 X. Cai, X. Jia, W. Gao, K. Zhang, M. Ma, S. Wang, Y. Zheng, J. Shi and H. Chen, *Adv. Funct. Mater.*, 2015, **25**, 2520–2529.
- 36 X. Cai, W. Gao, M. Ma, M. Wu, L. Zhang, Y. Zheng, H. Chen and J. Shi, *Adv. Mater.*, 2015, **27**, 6382–6389.
- 37 L. Jing, *Theranostics*, 2016, **6**, 40.
- 38 M. Hu, S. Furukawa, R. Ohtani, H. Sukegawa, Y. Nemoto, J. Reboul, S. Kitagawa and Y. Yamauchi, *Angew. Chem.*, 2012, **124**, 1008–1012.
- 39 Y. Su, Z. Teng, H. Yao, S. Wang, Y. Tian, Y. Zhang, W. Liu, W. Tian, L. Zheng and N. Lu, *ACS Appl. Mater. Interfaces*, 2016, **8**, 17038–17046.
- 40 M. Ishizaki, K. Kanaizuka, M. Abe, Y. Hoshi, M. Sakamoto, T. Kawamoto, H. Tanaka and M. Kurihara, *Green Chem.*, 2012, **14**, 1537–1544.
- 41 A. Gotoh, H. Uchida, M. Ishizaki, T. Satoh, S. Kaga, S. Okamoto, M. Ohta, M. Sakamoto, T. Kawamoto and H. Tanaka, *Nanotechnology*, 2007, **18**, 345609.
- 42 M. Ishizaki, A. Gotoh, M. Abe, M. Sakamoto, H. Tanaka, T. Kawamoto and M. Kurihara, *Chem. Lett.*, 2010, **39**, 762–763.
- 43 M. Ishizaki, Y. Sajima, S. Tsuruta, A. Gotoh, M. Sakamoto, T. Kawamoto, H. Tanaka and M. Kurihara, *Chem. Lett.*, 2009, **38**, 1058–1059.
- 44 Y. Ma, Z. Dai, Z. Zha, Y. Gao and X. Yue, *Biomaterials*, 2011, **32**, 9300–9307.



45 Y. Ma, X. Liang, S. Tong, G. Bao, Q. Ren and Z. Dai, *Adv. Funct. Mater.*, 2013, **23**, 815–822.

46 W. Teng, J. Cappello and X. Wu, *J. Controlled Release*, 2011, **156**, 186–194.

47 C. M. Hessel, V. P. Pattani, M. Rasch, M. G. Panthani, B. Koo, J. W. Tunnell and B. A. Korgel, *Nano Lett.*, 2011, **11**, 2560–2566.

48 Q. Tian, F. Jiang, R. Zou, Q. Liu, Z. Chen, M. Zhu, S. Yang, J. Wang and J. Hu, *ACS Nano*, 2011, **5**, 9761–9771.

49 L. Catala, T. Gacoin, J. P. Boilot, É. Rivière, C. Paulsen, E. Lhotel and T. Mallah, *Adv. Mater.*, 2003, **15**, 826–829.

50 M. Yamada, M. Arai, M. Kurihara, M. Sakamoto and M. Miyake, *J. Am. Chem. Soc.*, 2004, **126**, 9482–9483.

51 T. Uemura, M. Ohba and S. Kitagawa, *Inorg. Chem.*, 2004, **43**, 7339–7345.

52 D. K. Roper, W. Ahn and M. Hoepfner, *J. Phys. Chem. C*, 2007, **111**, 3636–3641.

53 M. Kastantin, B. Ananthanarayanan, P. Karmali, E. Ruoslahti and M. Tirrell, *Langmuir*, 2009, **25**, 7279–7286.

54 A. K. Kenworthy, S. A. Simon and T. J. McIntosh, *Biophys. J.*, 1995, **68**, 1903–1920.

55 K. Yang, H. Xu, L. Cheng, C. Sun, J. Wang and Z. Liu, *Adv. Mater.*, 2012, **24**, 5586–5592.

